Essential Readings in Light Metals: Aluminum Reduction Technology.
Edited by Geoff Bearne, Marc Dupuis and Gary Tarcy.

Analysis of Magnetohydrodynamic Instabilities in Aluminum Reduction Cells

M. Segatz and C. Droste
VAW aluminium AG
53117 Bonn, Germany

Abstract

The growth rate, period of oscillation, and spatial shape of interface waves in Hall-Héroult cells are determined from a linear stability analysis in the three-dimensional domain of liquid bath and metal. The linearized Maxwell and momentum equations together with the demand for hydrostatic balance at the interface describe a self-exciting oscillator. The corresponding eigenvalue problem for the interface movement is solved numerically. The resulting periods of typically 20–40s are in good agreement with measurements.

Both the steady-state as well as the oscillating component of the three-dimensional magnetic field and current density pattern are included. This gives a consistent description of different instability-driving mechanisms.

The spatial distribution of the electromagnetic to kinetic energy transfer is used to localize the regions in the cell which mainly cause instabilities . The influences of current intensity, ACD, metal pad height, and density ratio on strength and type of instability are demonstrated.

Introduction

Magnetohydrodynamic (MHD) instability in Hall-Héroult cells is a physical phenomena caused by an intricated interaction between metal/bath interface deformation, current flow, and magnetic field. Periodic oscillations of the cell voltage in the range of 20-40 s are a typical indication of MHD instabilities, also called metal pad roll. The associated differences in motion between bath and liquid metal lower the current efficiency due to the increased turbulence in the interface boundary layer. Increasing the anode-cathode distance (ACD) usually suppresses MHD instabilities, but results in a higher cell voltage. Metal pad roll with large amplitudes can even lead to short-circuits between anode and cathode.

Avoidance of MHD instabilities is one of the keys to successful pot operation. The magnetic field and current distribution in the cell are obviously of great influence on the desired stability. Some explanations have been published using analytical and numerical approaches to describe the mechanisms causing MHD instabilities [1-10]. As a result very different criteria were presented to avoid instabilities. An overview of these criteria is given in [11, 12].

Linear stability methods, assuming a single plane wave as interface distortion, show some physical mechanisms resulting in MHD instabilities [4, 6, 9, 13]. Two types of instability are described, one originating from horizontal currents in the liquid metal and the other from gradients in the magnetic field.

The main disadvantage of applying these theories to real cells is the lack of appropriate lateral boundary conditions. The geometry of these models is of infinite horizontal size. The reflection of large scale waves at the ledge should produce standing waves, resulting from the superposition of propagating waves with opposite direction and same amplitude, wave length and oscillation period. A positive growth rate of the amplitude of a wave propagating in one direction implies damping of the other wave travelling in the opposite direction. Thus the instability of waves with a wavelength similar to the size of the cell is not explained by these theories.

Other numerical approaches use a wave equation based on the shallow depth approximation [1, 2], or a direct time-integration of the transient equation of motion [8, 10]. Another semi-dynamic model of the cell [3] simulates a rotating interface wave, as has been observed in many instances, e.g. [14, 15]. The methods based on time-integration are computing intensive and are not applicable in an interactive development environment. Other authors usually neglect the effect of the magnetic field oscillations.

An interface wave is accompanied by changes of the current density, that always changes the magnetic field present. These magnetic field oscillations are of significant amplitude, as has been measured and calculated [15, 16]. Therefore their influence on the Lorentz forces should be considered in a cell model, especially if steady-state horizontal currents are present. A procedure including the effects of the three-dimensional steady-state and transient magnetic field and current density distribution is needed to predict the tendency of cells to MHD instabilities in a general manner. A mathematical model allowing such an analysis will be presented in the next section.

Mathematical Model

The geometry of the underlying model of the Hall-Heróult cell consists of a rectangular box with three horizontal layers representing the liquid metal, bath and anodes, c.f. Figure 1. The horizontal size of the box is $x_l \times y_l$, with the origin of the $x-$ and $y-$axis

located at the centre of the cell. The flat metal/bath interface is located at $z=0$, and the z-axis is directed upward. The heights of the liquid metal, bath and anodes are z_m, z_b, and z_a.

Electric potential and current density are defined in the entire cell model. Thus the effect of the anodic voltage drop on the distribution of the current density in the metal and bath is included. Pressure, velocity, magnetic flux and Lorentz force are considered in the liquid metal and bath only.

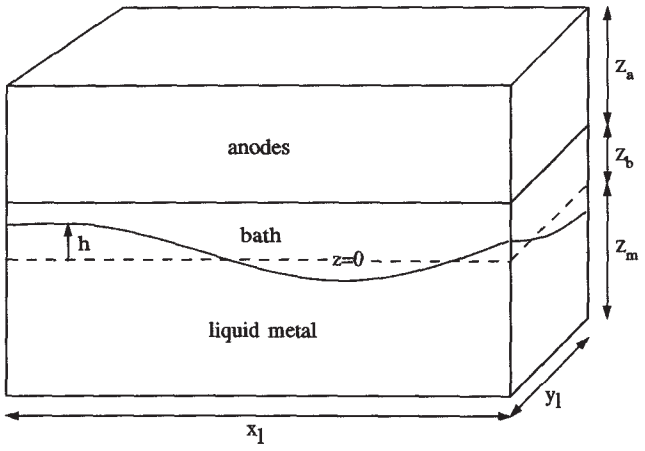

Figure 1: Geometry of the cell model.

The cathode block is not included in the model because of the high ratio between the electrical conductivity of the liquid metal and cathode carbon. It is assumed that the current entering the cathode block is not modified by MHD instabilities.

The cell model is meshed with $n_x \times n_y$ horizontal divisions and with n_{zm}, n_{zb}, and n_{za} vertical divisions in the liquid metal, bath and anodes. In principle, it is not necessary to use a uniformly spaced horizontal mesh. In this way for example the geometry of the centre gap between the anodes could be taken into account. However, the utilization of symmetry when using a regular mesh reduces the computing time significantly, especially for the determination of the magnetic field. The examples presented here are based on regular meshes.

According to the linear stability theory, all relevant physical field quantities in our model are separated into a steady-state and transient part. The steady-state components, denoted by capital letters, describe a consistent physical system which has no variation in time. The lower-case perturbed portions are assumed to be harmonic functions of time:

$$\begin{array}{lrcl} \text{interface deformation} & = & H & + \; h\, e^{st} \\ \text{pressure} & = & P & + \; p\, e^{st} \\ \text{electric potential} & = & \Phi & + \; \phi\, e^{st} \\ \text{velocity} & = & \mathbf{U} & + \; \mathbf{u}\, e^{st} \\ \text{current density} & = & \mathbf{J} & + \; \mathbf{j}\, e^{st} \\ \text{magnetic flux} & = & \mathbf{B} & + \; \mathbf{b}\, e^{st} \\ \text{Lorentz force} & = & \mathbf{F} & + \; \mathbf{f}\, e^{st} \end{array} \qquad (1)$$

The field components are defined in three-dimensions in the liquid bath and metal, with exception of the two-dimensional metal/bath interface deformation. The harmonic field amplitudes can be complex to allow for phase shifts. The complex parameter $s = s_r + \imath s_i$ describes the time development of the oscillations. The imaginary part corresponds to the oscillation period T with $s_i = 2\pi/T$. The growth rate, $s_r > 0$, or damping rate, $s_r < 0$, of an instability is given by the real part of s. The term 'unstable oscillation' will be used in conjunction with a positive growth rate, a 'stable oscillation' denotes a vanishing or negative growth rate.

We will follow here the approach of Sneyd [4]. The linearized equation of motion for the perturbed quantities in the liquid bath and metal is

$$\nabla p = \mathbf{f} - \rho s \mathbf{u}, \qquad (2)$$

where the density ρ is equal to ρ_m in the liquid metal and ρ_b in the bath. Influences of the steady-state velocity $\mathbf{U}$ and the viscosity of the fluids are neglected. Together with the continuity equation for an incompressible fluid

$$\nabla \cdot \mathbf{u} = 0, \qquad (3)$$

the pressure p fulfills the Poisson equation

$$\Delta p = \nabla \cdot \mathbf{f}. \qquad (4)$$

The linearization allows a direct determination of the divergence of the Lorentz forces. The first order terms of the Lorentz force are

$$\mathbf{f} = \mathbf{j} \times \mathbf{B} + \mathbf{J} \times \mathbf{b}. \qquad (5)$$

The magnetic flux $\mathbf{B}$ includes the magnetic effect of the external busbar system, the magnetized steel parts and the steady-state current distribution $\mathbf{J}$ in the liquid bath and metal. The perturbed magnetic flux $\mathbf{b}$ is caused by the current fluctuations in the bath and metal $\mathbf{j}$ and in the anodes. The Maxwell equations

$$\nabla \times \mathbf{B} = \mu \mathbf{J}, \qquad \nabla \times \mathbf{b} = \mu \mathbf{j}, \qquad (6)$$

allow the simplification of the divergence of the Lorentz force as

$$\nabla \cdot \mathbf{f} = -2\mu\, \mathbf{J} \cdot \mathbf{j}. \qquad (7)$$

It should be mentioned here that the magnetic field $\mathbf{b}$ is generated not only from the currents in the liquid bath and metal but from the current variations in the anodes and studs as well. The magnetic field of the current fluctuations in the studs is incorporated by assuming the same vertical current as in the anodes.

The steady-state and transient current density have to be determined in the complete cell model from Ohm's law $\mathbf{J} = -\sigma \nabla \Phi$ and $\mathbf{j} = -\sigma \nabla \phi$, where the electrical conductivity σ is equal to σ_m in the liquid metal and σ_b in the bath. The electric potential fulfills the Laplace equation

$$\Delta \Phi = 0, \qquad \Delta \phi = 0. \qquad (8)$$

Currents induced by the movement of the fluids or due to the transient magnetic flux are neglected because the magnetic Reynolds number is very small [17, 18]. The induced currents have a damping effect on instabilities, which is similar to the internal friction due to the viscosity. Our model will therefore overestimate the onset of instabilities.

Equation (8) requires the specification of appropriate boundary conditions at the bounding surfaces of both fluids. The ratio of

electrical conductivities in the cell suggest the assumption of a fixed electric potential at the top of the anodes for both the steady-state and transient term, and a prescribed steady-state current flow into the cathode block, while the transient currents do not enter the cathode block. Cold anodes can be simulated by a non-uniform resistance in the anode layer, sludge by prescribing an appropriate steady-state current density into the cathode block.

Linearization of Φ with respect to the perturbed interface gives a discontinuity in Φ at $z = 0$. Therefore the potential Φ is written as Φ_m and Φ_b. The complete set of boundary conditions for the perturbed electric potential are then as follows [9]:

$$\begin{aligned}
\phi &= 0 && \text{at} \quad z = z_b + z_a \,, \\
\sigma_b \frac{\partial \phi_b}{\partial z} &= \sigma_m \frac{\partial \phi_m}{\partial z} && \text{at} \quad z = 0 \,, \\
\phi_b - \frac{h}{\sigma_b}\frac{\partial \Phi}{\partial z} &= \phi_m - \frac{h}{\sigma_m}\frac{\partial \Phi}{\partial z} && \text{at} \quad z = 0 \,, \\
\frac{\partial \phi}{\partial z} &= 0 && \text{at} \quad z = -z_m \,, \\
\frac{\partial \phi}{\partial n} &= 0 && \text{at the ledge.}
\end{aligned} \tag{9}$$

For a given interface deformation the solution of equations (6) and (8) subject to the boundary conditions (9) defines the current density, magnetic field and Lorentz forces.

The boundary conditions for the Poisson equation for the pressure (4) can be derived from equation (2) at the boundaries of the metal and bath domain. An additional relation derives from the linearized hydrostatic balance at the interface,

$$\overline{\rho} g h = \overline{p} \qquad \text{at} \quad z = 0, \tag{10}$$

where $\overline{\rho}$ is the difference in densities and $\overline{p} = p_m - p_b$ is the discontinuity of the pressure at $z = 0$. Together with the linearized kinematic boundary condition of the interface $u_z = sh$ the normal component of the pressure gradient at the boundaries of the liquid metal and bath becomes

$$\begin{aligned}
\frac{\partial p}{\partial n} &= f_n && \text{at the outer boundary,} \\
\frac{\partial p}{\partial z} &= f_z - s^2 \frac{\rho}{\rho g}\overline{p} && \text{at the interface.}
\end{aligned} \tag{11}$$

In matrix notation, the equations (4) and (11) describe a general algebraic eigenvalue problem for the pressure p. This can be transformed to a standard eigenvalue problem for the pressure jump $\overline{p}$ across the interface. Due to its two-dimensionality, the size of the standard eigenvalue problem is reduced significantly.

The discretization of (4) with the source term (7) and boundary condition (11) will usually violate Green's theorem slightly. This has to be corrected to avoid an improper mass balance. Furthermore it is a necessary requirement for conservation of metal and bath volume to decrease the number of eigenmodes to $n_x \times n_y - 1$.

A larger problem arises from the necessity to calculate the magnetic field $\mathbf{b}$ in the bath and metal from the current density $\mathbf{j}$. Although the Lorentz forces and thus the magnetic field appear only at the boundary of the model, a complete determination of the Lorentz forces in the whole cell is desirable. This allows, for example, the analysis of the spatial distribution of the energy transfer into the cell, as will be demonstrated in the example sections. For a typical mesh with $n_x = 16$, $n_y = 12$, and $n_{zm} = n_{zb} = 4$, the number of Biot-Savard integrations is of the order 10^9. Efficient coding and utilisation of symmetries facilitates the handling of this problem.

The steady-state magnetic field generated by the external busbar system and by the internal currents in the liquid bath and metal, $\mathbf{B}$, is calculated on the three-dimensional mesh covering the volume of both fluids. The magnetic shielding of the steel shell has been taken into account [19].

The solved eigenvalue problem allows a further analysis of each eigenmode. The eigenvectors representing the pressure jump at the interface are transformed into an interface deformation. The scaling of the amplitude can be chosen arbitrarily. Normalization of the amplitude to a total energy of $1Nm$ gives typically a few millimetres in amplitude for the wave.

The velocities in the liquid metal and bath can be obtained from equation (2). The real part of the scalar product of the velocities and Lorentz forces gives the distribution of the magnetic energy converted to kinetic energy. Time-averaging of the converted energy , which has twice the frequency of the eigenmode, and integration over the volume of liquid bath and metal determines the rate of energy transferred into the cell. Decomposition of the Lorentz force into parts caused by the components of $\mathbf{B}$ and $\mathbf{J}$ and calculation of the individual contributions to the energy transfer allows the study of their influence on cell stability.

The variation of cell voltage can be calculated from the interface deformation for different time steps by an electrical network representing the resistances in the anodes and bath. This procedure is non-linear with respect to the relationship between the interface deformation and the change in bath resistance. The resulting voltage drop usually includes higher order harmonics in time.

Results

The method described has been used for the design of new high amperage cells now operating in Russia [20]. For various configurations of the magnetic field and current distribution calculations were performed giving a detailed insight into the intricate interaction of forces related to MHD instabilities. To isolate effects which usually occur together, the analysis of stability using artificial magnetic fields and current distributions was very helpful.

The following section will give a comparison of the method applied here and analytical solutions. Two examples of MHD instabilities, representing the main mechanisms, will be analyzed in more detail. The comparison of measurements and calculations of an instability observed for a reduction cell are also presented.

Verification

Without Lorentz forces the solution of the eigenvalue problem should yield the periods of the pure gravity wave. For a mode with m and n numbers of nodes in the longitudinal and transversal direction of the cell, respectively, the analytical solution of the oscillation period can be derived from an equation given for example

in [1]. Table I compares some periods of gravity oscillations for a cell with $lx = 8\,m$, $ly = 3.6\,m$, $z_m = 0.22\,m$ and $z_b = 0.05\,m$. The number of mesh points is $n_x = 15$, $n_y = 15$, and $n_{zm} = n_{zb} = 4$. The agreement between analytical and numerical results for pure gravity waves indicate the correct numerical representation of equation (2) in the limit of vanishing Lorentz forces.

Table I: Comparison of analytical and numerical oscillation periods (in seconds) for pure gravity waves and those modified by a vertical current. m and n are the number of nodes in lateral and transversal directions.

	pure gravity wave		modified gravity wave	
m, n	analytical	numerical	analytical	numerical
1,0	81.8	81.9	42.4	43.9
2,0	40.9	41.2	31.6	32.1
0,1	36.8	36.9	29.6	30.1
1,1	33.6	33.7	27.8	28.2
3,0	27.3	27.5	23.9	24.4
4,0	20.5	21.1	19.0	19.5
5,0	16.5	17.0	15.6	16.3

Another test was performed which included the effect of a homogeneous vertical current density $\mathbf{J}$. An analytical solution of the dispersion relation for a lateral infinite geometry is given in [9]. If the magnetic field $\mathbf{B}$ is assumed to be constant in z-direction, the period of the oscillations is influenced only by the magnitude of the vertical current density [21].

The numerical model was adapted to this situation by omitting the Lorentz forces at the lateral boundaries. The analytical solution does not include the anode region, so the anodic conductivity was assumed to be ten times of that of the liquid metal. The choice of $\mathbf{B}$ is not critical in this case. Only the vertical Lorentz forces enter the eigenvalue problem at the upper and lower boundaries of the liquid zones. Their influence on the oscillation is minor.

For typical current densities of about $0.7 A/cm^2$, the agreement between analytical and numerical solution is similar to that for the pure gravity wave, Table I. It is remarkable that the influence of the vertical current cuts the period of the (1,0)-wave in half.

Types of Instability

In principle, there are two self-exciting mechanisms which can force MHD instabilities, c.f. Figure 2. One is caused by the interaction of the currents $\mathbf{j}$ due to the oscillation with the steady-state magnetic field $\mathbf{B}$, called here 'type 1'. The magnetic field perturbation $\mathbf{b}$ together with the steady-state current distribution $\mathbf{J}$ forms another mechanism, 'type 2'. In general, both mechanisms act together resulting in a superposition of the Lorentz forces $\mathbf{f}_1$ and $\mathbf{f}_2$. The kinetic energy transferred into the cell can be quantified according to the type 1 and type 2 mechanism.

Assuming a homogeneous vertical current density and an instability forcing magnetic field situation, it is much more likely that the type 1 mechanism is dominant, because of the relative small values of $\mathbf{b}$. On the other hand, for a current disturbance in $\mathbf{J}$ the type 2

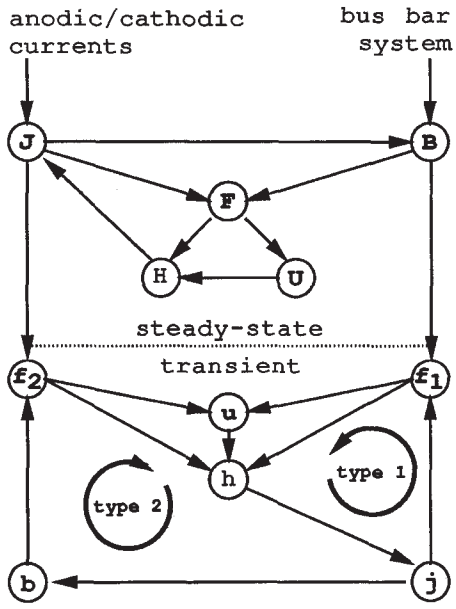

Figure 2: The self-exciting mechanisms of the instabilities ($\mathbf{J}$, $\mathbf{j}$: current density; $\mathbf{B}$,$\mathbf{b}$: magnetic field; $\mathbf{U}$,$\mathbf{u}$: velocity; $\mathbf{f}_1$,$\mathbf{f}_2$: Lorentz forces; H,h: interface deformation).

mechanism could dominate the instabilities. However, the disturbance in $\mathbf{B}$ due to $\mathbf{J}$ often enables a significant type 1 mechanism as well.

The main question here is under which conditions of $\mathbf{J}$ and $\mathbf{B}$ will the type 1 and 2 mechanisms establish a self-exciting oscillator. It has been mentioned that a single standing wave, even if modified by Lorentz forces, cannot be unstable. However, the superposition of two different standing waves with a phase shift allows interacting forces to come into play resulting in a positive growth rate for both waves. Mathematically this corresponds to the fact that if in the algebraic system two real eigenvalues of two standing waves degenerate, the formation of a complex eigenvalue is possible.

The complex eigenvalues of the algebraic eigenvalue problem considered here are associated with complex eigenvectors. Therefore, the interface deformation of instability modes must include phase differences. Accordingly, the maximum deformation of the interface appears at different times at different positions. Thus, the unstable oscillations form propagating wave crests. In contrast, oscillations with a vanishing growth rate appear as deformed standing waves.

A general classification of instabilities of real cells can be achieved by analyzing the development of instabilities with increasing current density. Successive calculations of the eigenmodes at increasing current loads give a continuous path of eigenmodes. The appropriate magnetic field $\mathbf{B}$ has to be recalculated for each current step. The growth rate s_r of the eigenmodes is shown on the left hand side and the corresponding oscillation periods T on the right hand side of Figure 3 for current intensities between 0 kA and 165 kA.

At low currents the oscillation periods show values of those of pure gravity modes, as given in Table I. At this point the standing waves can be classified with the number of nodes in each direction.

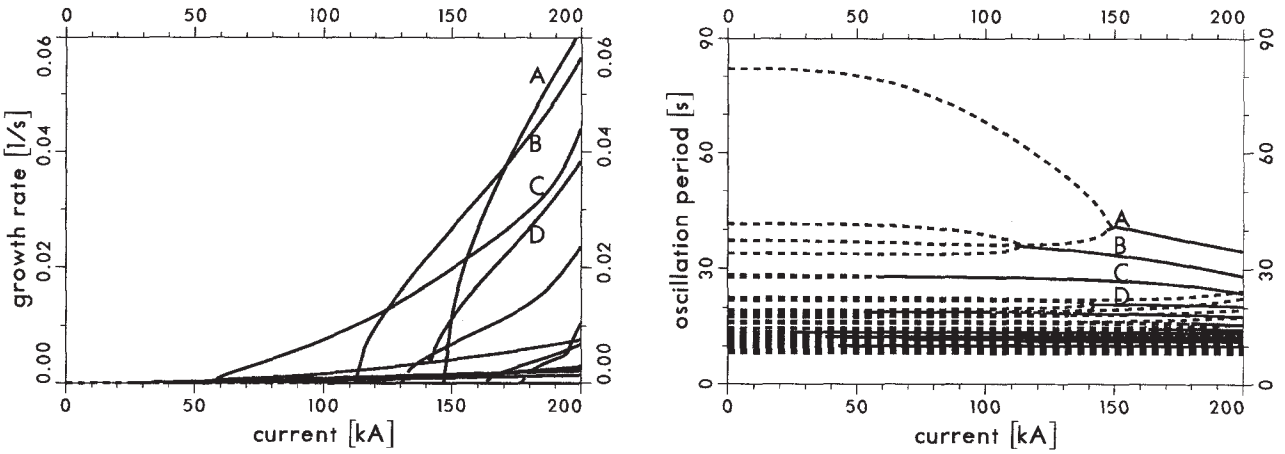

Figure 3: MHD instabilities as a function of current intensity. The letters A to D mark four different instabilities (solid lines), while stable oscillations appear as dashed lines.

With increasing current more and more modes tend to become unstable. A growth rate of 0.01 $1/s$ means the doubling of the amplitude of the interface deformation within about one minute. Accordingly the metal pad roll could develop inside a couple of minutes.

The increasing Lorentz forces deform the standing waves to change their shape and period in a complicated manner. Just before two stable waves become unstable, their period and shape are nearly identical. A rotating wave with a single wave crest, for example, marked A, originates from the $(1,0)$ and $(0,1)$ waves. The oscillation period of unstable waves tends to decrease with increasing current.

It is remarkable that the dependency of the growth rates on the current intensity varies. The Lorentz forces are proportional to the square of the current density, which might explain the more than linear increase in the growth rates with current intensity. An upper limit in the current load allowing stable operation can be derived, if the threshold of the growth rate, which accounts for friction, can be estimated.

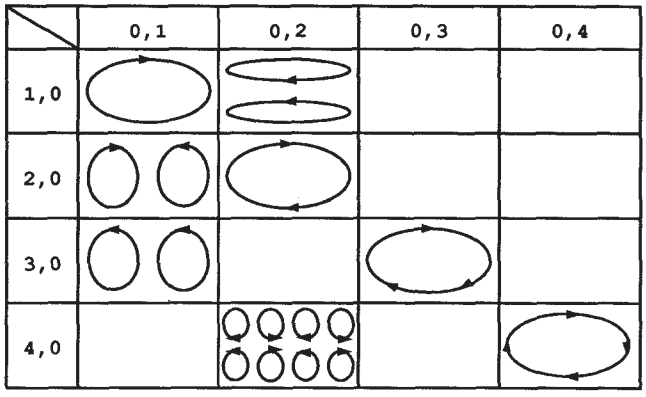

Figure 4: Propagation of wave crests for some instabilities classified according to their originating standing waves. Each arrow marks a wave crest.

Figure 4 illustrates essentially the propagation of wave crests for some instabilities, which originate from the standing waves denoted at the top and at the left hand side. Each arrow represents a single wave crest. It must be noted that the appearance of the interface deformation can be very different from the scheme shown in Figure 4, if, for example, the symmetry of the magnetic field is disturbed.

Influence of operational parameters

Parameters like metal height, ACD, and bath density, which are directly connected to pot operation procedures, have a large impact on cell stability. Although the principle effect of these parameters on stability is obvious, it will be analyzed here to give a quantitative measure.

The cell under consideration is identical to the example analyzed in more detail in the next section. While we will focus here on the principle influence of operational parameters on the stability, the next section will analyze the instabilities themselves.

The influence of the metal pad height on MHD instabilities is shown in Figure 5. An increasing metal height stabilizes the cell significantly. This is mainly due to the decreasing horizontal current density $\mathbf{j}$ in the metal. It is remarkable that most instabilities show a change in metal height dependence at 15–20cm, which are a typical values for real cells. Below this metal height, a sharp increase in the growth rate is seen. The period of stable oscillations decreases with metal pad height in an asymptotic manner. This is typical for pure gravity waves as well. In contrast, the characteristics of the largest unstable oscillations show an increase in the period with metal pad height.

Figure 6 shows the dependency of instabilities on the ACD. A strong decrease of the growth rate with increased ACD reflects the fact that the first response of the process control systems to noisy cells is usually an increase in the cell voltage by moving up the anode beam. The mode with the largest oscillation period (A) is unstable

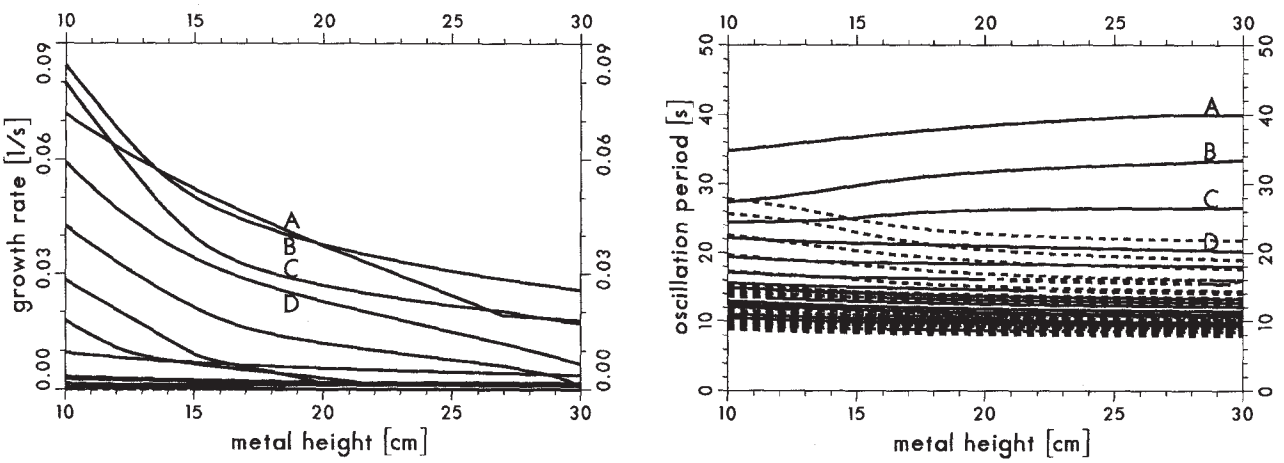

Figure 5: Growth rate and period of oscillations as function of liquid metal height. Unstable oscillations are drawn with solid, stable oscillations with dashed lines.

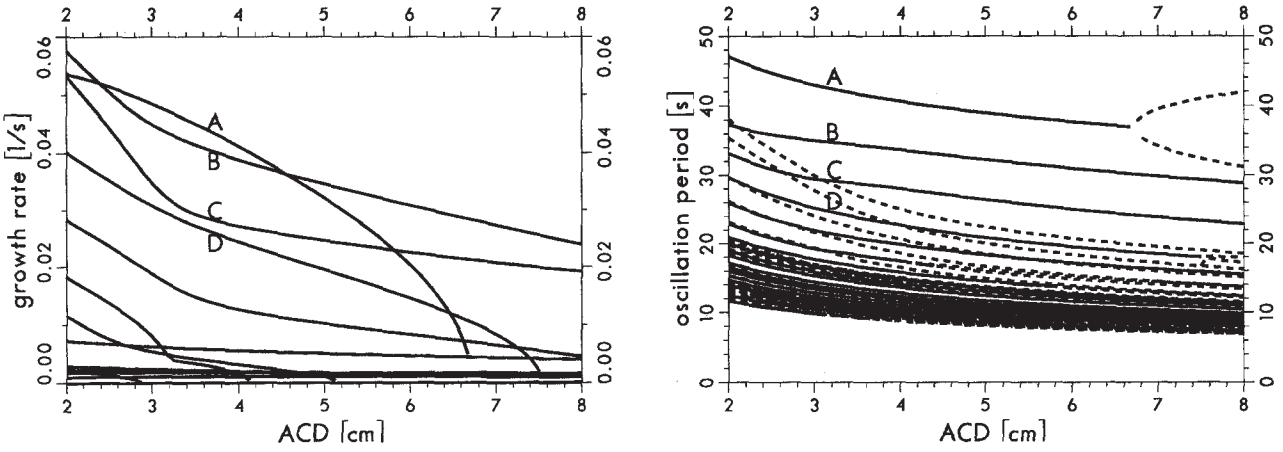

Figure 6: Growth rate and period of oscillations as a function of ACD.

only below an ACD of 6.8 cm, and splits in two stable modes above this value. Thus, a slow change of the ACD could result in a discontinuous change of the oscillation period, if instabilities are present.

The bath density has a large impact on the stability as well. Keeping the density of the liquid metal constant at $\rho_m = 2250\ kg/m^3$, the bath density was modified between $\rho_b = 1950\ kg/m^3$ and $2200\ kg/m^3$. A general trend towards higher instability with increasing bath density is to be expected and was found. At a bath density of about $2100\ kg/m^3$, some of the larger modes show a sharp increase towards higher instabilities with increasing bath densities. The oscillation periods become longer with increasing bath density, similar to the behaviour of pure gravity waves.

Example 1: Instability caused by external magnetic field

The prebaked, point-feeder cell discussed in this example has a symmetric busbar design with a current of $165\,kA$. Due to the adjacent pot line, the vertical magnetic field of this magnetic uncompensated cell has an offset of $20\,G$. An analysis of MHD stability is performed with a uniform vertical current distribution in the bath and metal. The deformation of the interface caused by the instability with the largest growth rate is shown in Figure 7. This oscillation is marked in Figures 3, 5, and 6 with (A). The real and imaginary part of the amplitude h of the interface deformation describe the complete time development of the wave. A whole oscillation cycle is given by a sequence of the real part, the negative imaginary part, the negative real part, and finally the imaginary part of the interface deformation.

The wave can be characterized by a single wave crest and trough rotating in a counterclockwise direction, as indicated by the arrows. However, the shape of the wave is not as simple as a pure superpo-

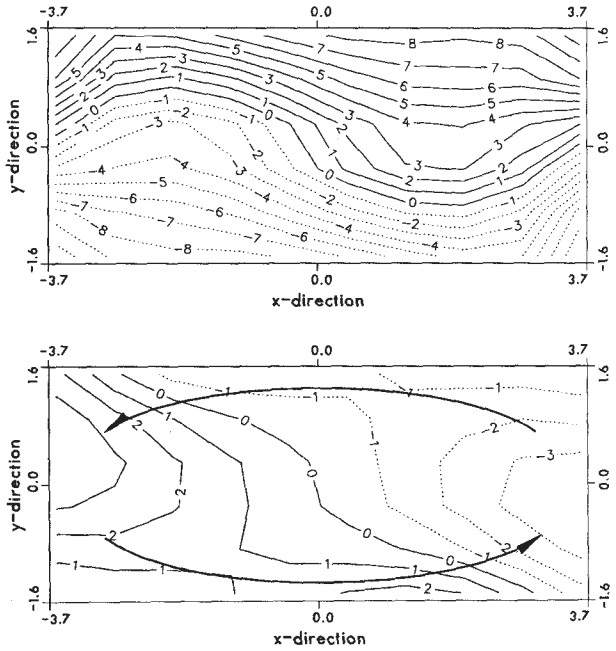

Figure 7: Real (top) and negative imaginary part (bottom) of the deformation h of the bath/metal interface (example 1): Heights are in millimeter. The arrows indicate the direction of propagation of the wave crest and trough.

sition of the (1,0) and (0,1) standing waves. The potential energy of the real part of h is much larger than the corresponding energy of the imaginary part. This reflects the cyclic exchange between potential and kinetic energy, which is largest for pure standing waves and decreases, as s_r increases.

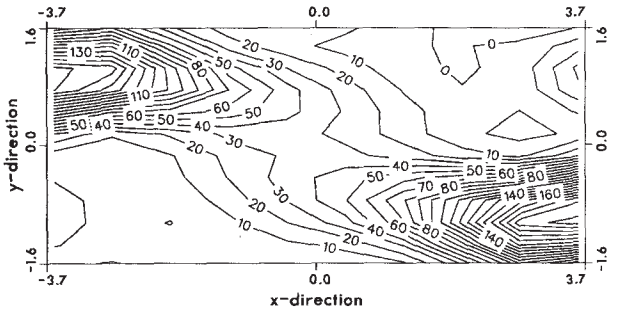

Figure 8: Kinetic energy density transferred into the liquid metal (example 1). Contour values are in units of mW/m^3.

The spatial distribution of the kinetic energy transferred into the cell in the mid-plane of the liquid metal is shown in Figure 8. Practically all energy is transferred due to the type 1 mechanism. The largest energy transfer is located close to those two corners where the positive offset of the vertical magnetic field, due to the adjacent pot line, superposes with the positive vertical field of the cell.

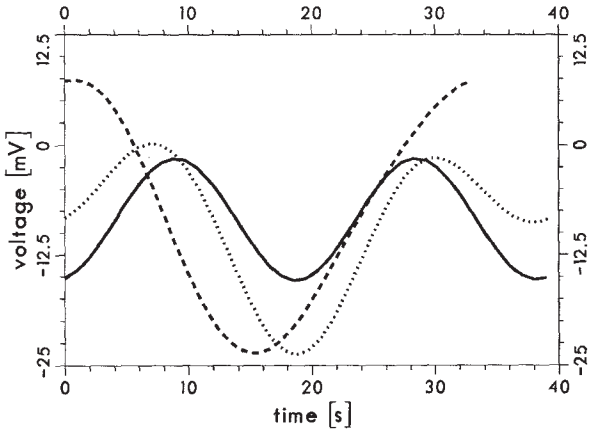

Figure 9: Cell voltage variation for uniform anode currents (solid line), cold middle anode (dotted line), and cold corner anode (dashed line).

With this picture in mind appropriate modifications to the busbar system can be developed.

Figure 9 shows the calculated fluctuation of the cell voltage in the time interval of one oscillation period with three different assumptions concerning the anodic configuration. The voltage fluctuations for a flat interface is zero. The solid line reflects a uniform anode current distribution with the same mean current intensity at all anodes. The oscillation period of the voltage is half the period of the eigenmode, because the single wave crest maximizes its amplitude at two corners during a cycle as can be seen in Figure 7. The voltage deviation is always negative due to the nonlinear change in local bath resistance with interface deformation.

A cold anode in the cell, a typical situation after an anode change, with half the mean current intensity modifies the variation of the cell voltage significantly. Located in the middle of the cell a cold anode gives an oscillation period of about $40\,s$ for the eigenmode, which is nearly the same as for those with a uniform anode current. The voltage variation shows a large and a small minimum as a function of time. With a cold corner anode on the left downstream side, the oscillation period of the eigenmode and of the voltage fluctuation are both $33\,s$. Although the three different waves are normalized to a total energy of $1\ Nm$, the wave amplitude height for the case of the cold corner anode is up to $15\ mm$, while only $11\ mm$ for the two other cases.

The large differences in the form of voltage fluctuation, are a result of the nonlinear relationship between the interface deformation and the resistance network. This allows the occurrence of higher frequencies in the voltage signal than in the eigenmode frequency. The positive deviation of the voltage for the cold corner anode indicates the moment when the wave crest is below the cold anode.

Variations in the cell voltage can be very small if the height of the crest is constant and if the mean anode currents are uniform. This type of oscillation can be detected only by measurement of individual anode or cathode currents, as described in [22], or by measuring the magnetic field variations.

Figure 9 demonstrates that the analysis of the variation of measured voltage fluctuations could give valuable information about the cause of an instability.

Example 2: Instability caused by cathodic current disturbance

In this example, a disturbance of the current density distribution in the liquid metal due to sludge on the cathode block is analyzed. To simulate this, the current density flow into one third of the cathode block on the downstream side of the cell is assumed to be zero simulating a large area of muck. The current density **J** is mainly horizontal in the liquid metal above the muck. It generates an additional magnetic field mainly on the long sides of the cell in the vertical direction, which adds up to **B**. An asymmetric busbar system is chosen to compensate for the offset in the vertical magnetic field due to the adjacent pot line.

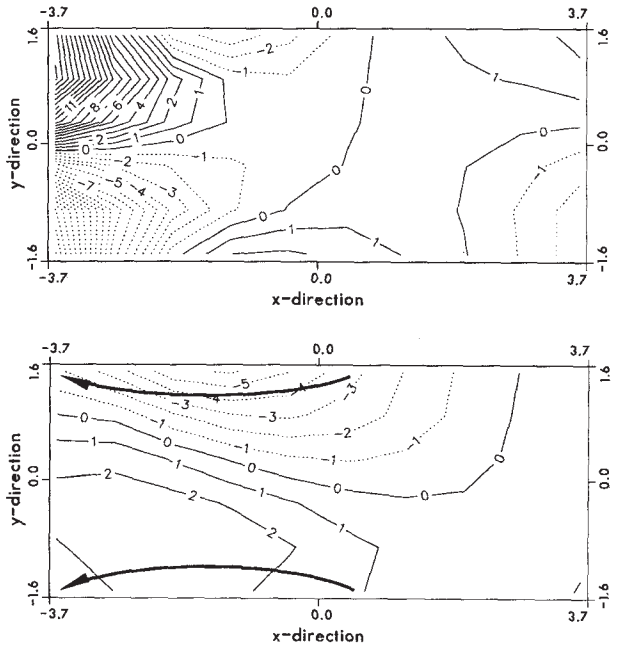

Figure 10: Real (top) and negative imaginary part of the interface deformation (bottom) with sludge assumed on the left third of the cell (example 2). Heights are in millimeter. The arrows indicate the path of propagating wave crests and troughs.

The largest instability mode, Figure 10, shows two wave crests alternately travelling in the upstream direction. The amplitude of the crests increase towards the short side of the cell by up to $20\,mm$. The propagation of the waves and the horizontal currents in the liquid metal have opposite direction. This phenomena is in agreement with the analysis in [6], which predicts the same direction of propagation for plane waves in the instance of a horizontal current.

The predominant portion of the kinetic energy transferred into the cell , about 99 %, is produced in the liquid metal. Table II separates the total transferred energy into the components caused by the different terms of the Lorentz forces. The energy input into the

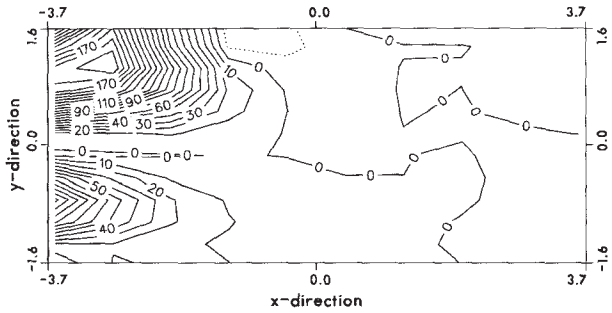

Figure 11: Magnetic to kinetic energy transfer for the type 1 instability (example 2). Contour values are mW/m^3.

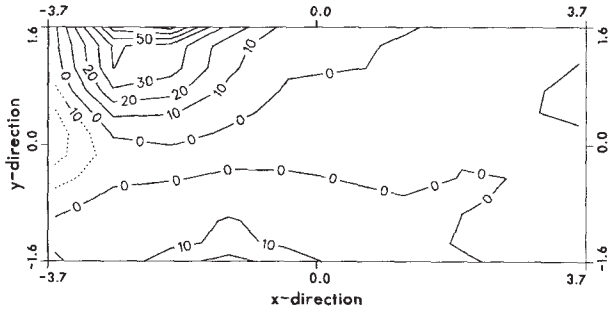

Figure 12: Magnetic to kinetic energy transfer for the type 2 instability (example 2). Contour values are mW/m^3.

cell in the mid-plane of the liquid metal is shown in Figure 11 for the type 1 and in Figure 12 for the type 2 mechanism. The first one, caused by the magnetic field **B**, has larger values than the latter, caused by **J**. The same fact is reflected by the volume-integrated values of the energy input. The energy transfer takes place mainly in the left downstream corner of the cell. At this location there is a superposition of the energy change originated from the circulating wave due to B_z and the wave due to the horizontal currents.

Table II: Percentage of kinetic energy transferred into the cell broken down into different terms contributing to the Lorentz force.

$B_x(j_z u_y - j_y u_z)$	-10.6%
$B_y(j_x u_z - j_z u_x)$	0.7%
$B_z(j_y u_x - j_x u_y)$	92.1%
$J_x(b_y u_z - b_z u_y)$	21.7%
$J_y(b_z u_x - b_x u_z)$	0.0%
$J_z(b_x u_y - b_y u_x)$	-3.9%

It was noticed that the current disturbances caused by either a non-uniform anodic current or cathodic current generate similar waves if the steady-state, horizontal current distribution and magnetic field in the liquid metal are similar. This is not obvious because the boundary conditions for the transient current density at the anode and cathode are different and the current density in the

bath is much more influenced by an anodic non-uniform current distribution than by a cathodic current disturbance.

Comparison with Measurements

Measurements, already published in [15], were used to analyze a cell instability. Individual anode currents, the cell voltage, and the magnetic field at the corner of the cell were logged for about $400\,s$. The harmonic oscillations in the magnetic field components indicated a typical MHD instability. The measured data are compared with the results of a stability calculation for the same cell.

Input for the numerical MHD analysis comprises the magnetic field $\mathbf{B}$, calculated from the busbar arrangement and the shielding of the steel shell, and an anode resistance distribution, which reflects the time-averaged non-uniform anode current distribution measured. The non-uniform anode resistances influence the shape and period of the instability only slightly, but they have a large impact on the voltage fluctuation. The amplitude of the wave was chosen to reflect best the magnitude of the measured cell voltage variation. This was achieved with an amplitude of the order of the ACD. Thus the bath resistance vanishes at the highest deformation of the interface and the current at this anode is limited by the anode resistance. The oscillation of the magnetic field was calculated at the position of the probe.

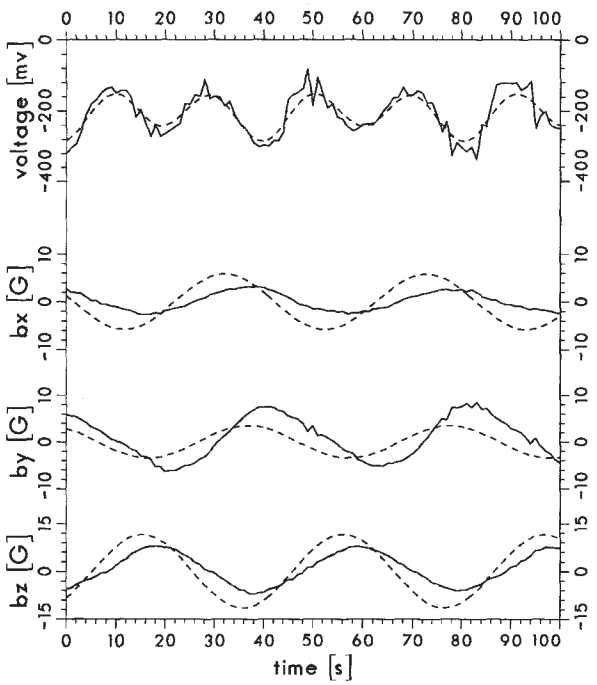

Figure 13: Comparison of the measured (solid) and calculated (dashed) cell voltage (top) and variation in magnetic field components b_x, b_y, and b_z (below) with time.

Figure 13 shows the measured and calculated cell voltage and magnetic field components as they vary with time. The oscillation periods are in good agreement. In particular the effect that the cell voltage shows a higher frequency spectrum than the magnetic field components is reflected in the calculations. The largest deviation between the measured and calculated data is the phase shift in the magnetic field components. This is probably due to varying additional currents in the vicinity of the probe, which have a strong influence on the measurement.

This comparison indicates that this linear stability model can simulate MHD instabilities very realistically. We think that the basic physics causing MHD instabilities are represented in our model in a correct manner.

Conclusion

A method to analyze the tendency towards MHD instabilities of real cells is presented. The effects of the three-dimensional steady-state and transient magnetic field and current density distribution are included giving a set of linearized equations describing the MHD physics.

In principle a MHD instability can be understood to be a superposition of two different standing waves with the same oscillation period and a non-zero phase shift between them. By changing the horizontal forces, one wave amplifies the other.

The interface deformation of an unstable oscillation must appear as propagating waves. A classification of the instabilities according to the standing waves, from which they originate, is possible. The self-exciting oscillator can be driven by two different mechanisms, which usually interact together. Rotating waves as well as waves travelling opposite to the direction of the horizontal current flow caused by a current perturbation in the cell are found.

The influence of metal pad height, ACD, and bath density on the tendency towards instability is in agreement with operational experience and practice. However the largest influence is definitely caused by the current intensity because of its nonlinear effect on the Lorentz forces.

Calculations have shown good agreement with the combined measurements of the voltage fluctuation and the magnetic field variation. Oscillation periods of the voltage fluctuation, easily acquired from the process control systems, can be predicted within this model. Analysis of periodic voltage fluctuations can be performed and compared with calculated voltage variations from the MHD model. Under certain circumstances it is already possible to determine whether a current disturbance or a magnetic field problem has caused the instability. A strong influence of anodic or cathodic current disturbances on the formation of instabilities is found. The growth rate, oscillation period and shape of the wave is a function of the type of disturbance.

The values for typical growth rates of instabilities are of the order of some $0.01\ s^{-1}$. Therefore, an exponential increase in the amplitude would require a couple of minutes to develop significant voltage fluctuations. This time scale is typical of observations on real cells.

The code analyzing the MHD instabilities has been incorporated into the integrated software package for the development of reduction cells [23], and allows an interactive determination and visualization of the stability situation and problem zones for a cell model.

References

[1] K. Mori, K. Shiota, N. Urata, and H. Ikeuchi, *The Surface Oscillation of Liquid Metal in Aluminum Reduction Cells*, Light Metals 1976, 77-95.

[2] N. Urata, K. Mori, and H. Ikeuchi, *Behavior of Bath and Molten Metal in Aluminium Electrolytic Cell*, Kaikinzoku (Light Metals, Japan), 26, 1976, 573-583.

[3] T. Sele, *Instabilities of the Metal Surface in Electrolytic Cells*, Light Metals 1977, 7-24.

[4] A.D. Sneyd, *Stability of Fluid Layers Carrying a Normal Electrical Current*, J. Fluid Mech. 1985, 223-236.

[5] N. Urata, *Magnetics and Metal Pad Instability*, Light Metals 1985, 581-591.

[6] R. Moreau and D. Ziegler, *Stability of Aluminum Cells - A New Approach*, Light Metals 1986, 359-364.

[7] J. Descloux and M.V. Romerio, *On the Analysis by Perturbation Methods of the Anodic Current Fluctuations in an Electrolytic Cell for Al*, Light Metals 1989, 237-243.

[8] V. Potocnik, *Modelling of Metal-Bath Interface Waves in Hall-Heroult Cells using ESTER/PHOENICS*, Light Metals 1989, 227-235.

[9] P.A. Davidson and R.F. Boivin, *Hydrodynamics of Aluminium Reduction Cells*, Magnetohydrodynamics in Process Metallurgy 1991, 111-116.

[10] M. Segatz, D. Vogelsang, C. Droste, and P. Baekler, *Modelling of transient magneto-hydrodynamic phenomena in Hall-Heroult cells*, Light Metals 1993, 361-368.

[11] A.F. LaCamera, D.P. Ziegler, and R.L. Kozarek, *Magnetohydrodynamics in the Hall-Heroult Process, an Overview*, Magnetohydrodynamics in Process Matallurgy 1991, 91-98.

[12] V. Potocnik, *Principles of MHD Design of Aluminium Electrolysis Cells*, Magnetohydrodynamics in Process Metallurgy 1991, 99-105.

[13] S. Pigny and R. Moreau, *Stability of Fluid Interfaces carrying an Electric Current in the Presence of a Magnetic Field*, European Jnl. Mech. B/Fluids 1992.

[14] S. Cherchi and G. Degan, *Oscillation of Liquid Aluminium in Industrial Reduction Cells: An Experimental Study*, Light Metals 1983, 457-467.

[15] G. Loßmann, *Utilization of various combined measurements in reduction cells for operational improvement*, Light Metals 1992, 441-447.

[16] R. Boivin and S. Martel, *Effect of an Instability of the Metal Surface on the Magnetic Field in a Cell*, Light Metals 1990, 233-241.

[17] K. Ai, *The Hydrodynamics of the Hall-Heroult Cell*, Light Metals 1985, 593-607.

[18] R. Moreau, and J.W. Evans, *An Analysis of the Hydrodynamics of Aluminum Reduction Cells*, J. Electrochem. Soc. Electrochemical Science and Technology (1984), vol. 131, no. 10, 2251-2259.

[19] M. Segatz and D. Vogelsang, *Effect of Steel Parts on Magnetic Fields in Aluminum Reduction Cells*, Light Metals 1991, 393-398.

[20] D. Vogelsang, M. Segatz, C. Droste, P.Baekler, and R. Stücher, *Development of a 300-kA Reduction Cell: Application of Simulation Tools for the Conceptual Design*, Light Metals 1994.

[21] Y. Fautrelle, *Free Surface Electromagnetic Instabilities in Liquid Metals*, Magnetohydrodynamics in Process Metallurgy 1991, 63-68.

[22] E. Matsui, *Measurement of Metal Turbulence in Aluminium Reduction Cells*, Light Metals 1982, 373-389.

[23] D. Vogelsang and M. Segatz, *Simulation Tools for the Development of High-Amperage Reduction Cells*, Light Metals 1991, 375-379.